SANDIA REPORT
SAND2021-12191
Printed August 2021

Sandia National Laboratories

Development of a Ductile Rupture Failure Surface for PH13-8Mo H950 Steel Using the Xue-Wierzbicki Failure Model.

Robert J. Kalan

Prepared by
Sandia National Laboratories
Albuquerque, New Mexico
87185 and Livermore,
California 94550

Issued by Sandia National Laboratories, operated for the United States Department of Energy by National Technology & Engineering Solutions of Sandia, LLC.

Available to DOE and DOE contractors from
U.S. Department of Energy
Office of Scientific and Technical Information
P.O. Box 62
Oak Ridge, TN 37831

Telephone:	(865) 576-8401
Facsimile:	(865) 576-5728
E-Mail:	reports@osti.gov
Online ordering:	http://www.osti.gov/scitech

Available to the public from
U.S. Department of Commerce
National Technical Information Service
5301 Shawnee Rd
Alexandria, VA 22312

Telephone:	(800) 553-6847
Facsimile:	(703) 605-6900
E-Mail:	orders@ntis.gov
Online order:	https://classic.ntis.gov/help/order-methods/

ABSTRACT

The ability to model ductile rupture in metal parts is critical in highly stressed applications. The initiation of a ductile fracture is a function of the plastic strain, the stress state, and stress history. This paper develops a ductile rupture failure surface for PH13-8Mo H950 steel using the Xue-Wierzbicki failure model. The model is developed using data from five tensile specimen tests conducted at -40°C and 20°C. The specimens are designed to cover a Lode parameter range of 0 and 1 with a stress triaxiality range from zero in pure shear to approximately 1.0 in tension. The failure surface can be implemented directly into the finite element code or used as a post processing check.

CONTENTS

LIST OF FIGURES

LIST OF TABLES

This page left blank

1. INTRODUCTION

Failure of metal parts by ductile rupture in highly stressed regions during energy limiting events is of concern in many engineering applications, Modeling the initiation of fracture under these conditions is essential to their safe design. This document discusses the development of a ductile rupture failure surface for PH13-8Mo H950 steel using the Xue-Wierzbicki failure model [1]. Five tensile test specimen types were used to generate the fracture data for the development of this model. The specimen types are shown in Figure 1 and drawings for the five types are presented in Appendix A. The specimens are designed to cover a Lode parameter range of 0 and 1 with a stress triaxiality range from zero in pure shear to approximately 1.0 in tension. Details of the specimen testing are discussed in Reference [2].

Figure 1. The test specimens are left to right: standard tensile (R5), flat groove, 9 mm notch, 3 mm notch, and shear specimens

Data for each specimen was obtained at -40^{o}C and 20^{o}C. The standard tensile test specimen meets the requirements of a R5 tensile bars from ASTM specification E8-16 [3] and will be referred to as the R5 specimen. The engineering stress-strain data from the R5 specimen is used to develop the true strain-curve. This curve is incorporated in the hydra plasticity model used in the finite element analyses. Finite element models were developed for each specimen and are used to determine the stress state and plastic strain at failure. Using the calculated stress state, a failure surface based on the Lode angle, the stress triaxiality, and the plastic strain is developed.

2. REVIEW OF DUCTILE RUPTURE AND THE XUE-WIERBICKI MODEL

The fracture process of ductile materials is known to be caused by the nucleation of voids at stress sites where compatibility of deformation is difficult such as inclusions and second-phase particles. This is followed by void growth and void coalescence. Coalescence occurs by elongation of the voids and elongation of the bridges of material between the voids. This leads to the development of a fracture surface.

Bridgman performed the seminal work on the effect of hydrostatic pressure on ductile rupture in the 1940's and 1950's [4]. He conducted over 350 tensile tests on 20 different types of steel of different heat treatments. These experiments show that the strain to fracture is an increasing function of the superposed hydrostatic pressure. This work was further developed by Johnson and Cook [5], who developed fracture models for OFHC copper, Armco iron, and 4340 steel using notched tensile specimens. Their model contained three primary terms; one with a dimensionless strain rate, one for dimensionless temperature and one with a dimensionless pressure-stress ratio $\eta = \frac{\sigma_m}{\bar{\sigma}}$ where σ_m is the average of the three normal stresses and $\bar{\sigma}$ is the von Mises equivalent stress. The pressure-stress ratio is commonly referred to as the stress triaxiality. Figure 2 shows a plot of the data developed by Johnson and Cook and the corresponding curves developed in their failure models.

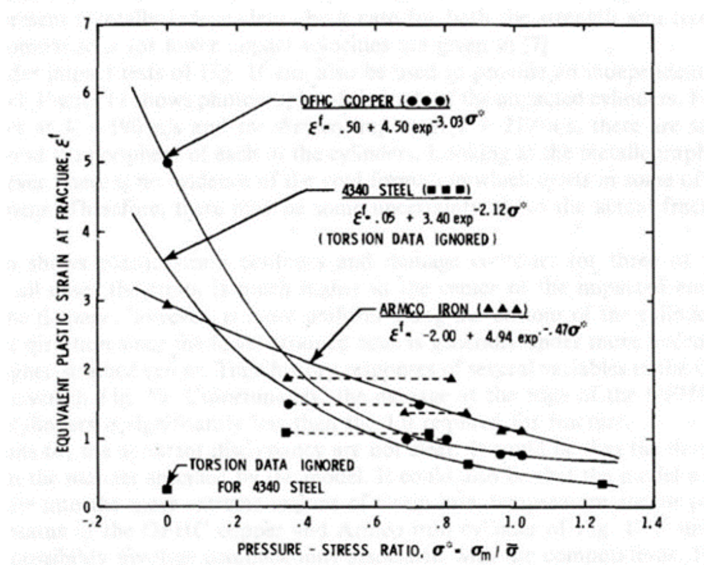

Figure 2. Plastic strain vs. stress triaxiality from Johnson and Cook [4].

Bao [6] developed a new criterion for ductile crack formation. This work is based on extensive testing on 2024-T351 aluminum. He developed a failure locus shown in Figure 3, in stress triaxiality-equivalent strain space, based on the calculating the average stress triaxiality as

$$\left(\frac{\sigma_m}{\bar{\sigma}}\right)_{avg} = \frac{1}{\bar{\varepsilon}_f}\int_0^{\bar{\varepsilon}_f} \frac{\sigma_m(\bar{\varepsilon})}{\bar{\sigma}(\bar{\varepsilon})}\, d\varepsilon. \quad (1)$$

Where $\bar{\varepsilon}$ is the equivalent strain and $\bar{\varepsilon}_f$ is the equivalent strain at fracture.

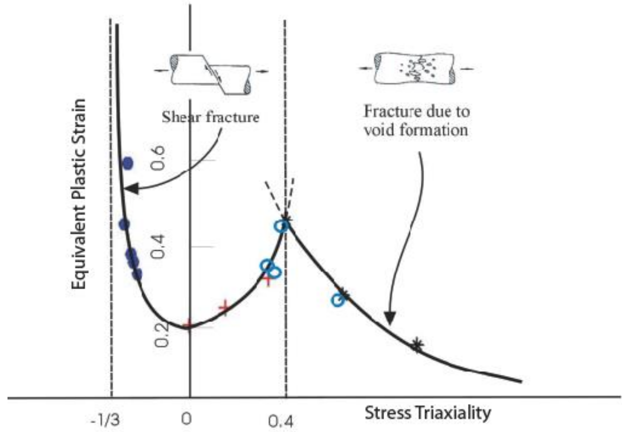

Figure 3. Stress failure locus of Al2024-T351 developed from Bao[5]

The anomalous torsional data point for 4340 steel in Figure 2 and the dip in the experimental data for aluminum shown in Figure 3, indicates that the failure strain in simple shear can be lower than the dimensionless pressure-stress ratio, η would indicate. This change can be accounted for by considering the Lode angle dependency of the loaded state [8][9].

The principal stress coordinates $(\sigma_1, \sigma_2, \sigma_3)$ can be used to characterize stress space. For isotropic materials the independence of the ordering of the three principal stresses provide a 120^{o} symmetry about the [1 1 1] (hydrostatic) direction. The Lode cylindrical coordinates offer an alternative cylindrical system [r, θ, z] for which the z- axis points along the hydrostatic <111> axis and [r, θ] are polar coordinates on any constant pressure (z) cross-section (Figure 4).

As shown in Figure 4, the cylindrical Lode coordinates may be determined from the stress invariants I_1, J_2, and J_3. Specifically,

$$r = \sqrt{2J_2}, \tag{2}$$

$$z = \frac{I_1}{\sqrt{3}}, \tag{3}$$

the Lode angle parameter ξ is related to the azimuthal angle θ defined in the octahedral plane by

$$\xi = \cos(3\theta) = \frac{27J_3}{2\bar{\sigma}^2} \tag{4}$$

Where the invariants are a mixture of the Cauchy stress σ , and the stress invariant s, and are given by

$$I_1 = \sigma_1 + \sigma_2 + \sigma_3 \tag{5}$$

$$J_2 = \frac{1}{2}[tr(\sigma^2) - \frac{1}{3}\, tr(\sigma^2) = \frac{1}{2} tr(s \cdot s) \tag{6}$$

$$J_3 = \det(s) \tag{7}$$

$$s = \sigma - \frac{1}{3}\, I_1 \tag{8}$$

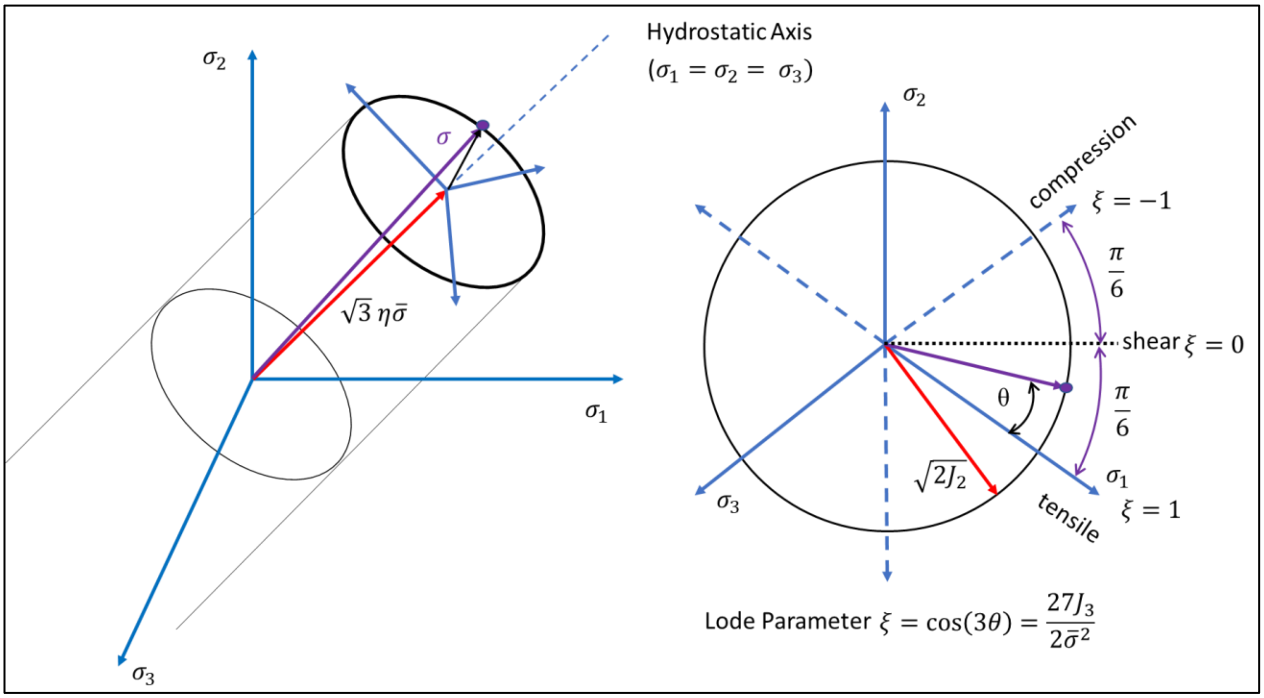

Figure 4 Lode parameter in principal stress space

In the Xue-Wierzbicki ductile failure model [8], the failure strain is defined by average values of the stress triaxiality and the Lode angle parameter as:

$$\bar{\varepsilon}_f = F(\eta_{avg}, \xi_{avg}) \tag{9}$$

$$\eta_{avg} = \frac{1}{\bar{\varepsilon}_f} \int_0^{\bar{\epsilon}_f} \eta(\varepsilon) d\varepsilon \tag{10}$$

$$\xi_{avg} = \frac{1}{\bar{\varepsilon}_f} \int_0^{\bar{\epsilon}_f} \xi(\varepsilon) d\varepsilon \tag{11}$$

Where ε is the total current plastic strain, and $\bar{\varepsilon}_f$ is the plastic strain at failure.

In the following discussion, average values of ξ and η will be used and the subscript "*avg*" will be dropped for the equations.

In stress triaxiality space, the fracture strain is bounded by the two curves $\xi = 1$ and $\xi = 0$. Experimental evidence [6] [8] (include this work) has shown that the stress state with $\xi = 1$ represent the condition for the highest ductility, while the stress state with $\xi = 0$ represent the least ductile state. This is shown schematically in Figure 5 which shows the fracture strain as a function of η for the two bounding values of ξ.

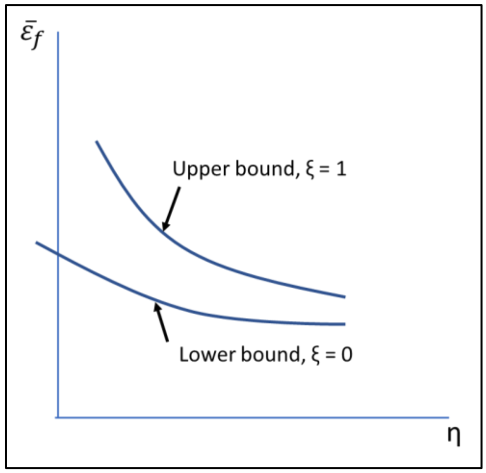

Figure 5 Schematic showing the upper and lower bound of failure strain dependence on the lode angle parameter

An exponential function is used to represent the two bounding curves,

$$\bar{\varepsilon}_f = C_1 e^{-C_2 \eta}, \quad \xi = 1 \tag{12}$$

$$\bar{\varepsilon}_f = C_3 e^{-C_4 \eta}, \quad \xi = 0. \tag{13}$$

Weirzibicki and Xue [1] assume that a family of elliptical functions can be used to describe the drop in fracture strain between the two limiting curves. This results in the following function which describes the failure strain in 3-D space $\{\bar{\varepsilon}_f, \xi, \eta\}$.

$$\bar{\varepsilon}_f = F(\eta, \xi) = C_1 e^{-C_2 \eta} - [(C_1 e^{-C_2 \eta} - C_3 e^{-C_4 \eta})](1 - \xi^m) \tag{14}$$

Where *m* is the even integer closest to *1/n* where *n* is the hardening exponent of the true stress strain curve.

3. DEVELOPMENT OF THE TRUE STRESS-STRAIN CURVE

The data from the R5 tensile specimens were used to develop an engineering stress-strain curve for the PH13-8Mo H950 steel. Six tests were run on each of the test specimens. Three specimens were tested at -40°C and three were tested at room temperature (20°C). The R5 engineering stress-strain data for -40°C is shown in Figure 6.

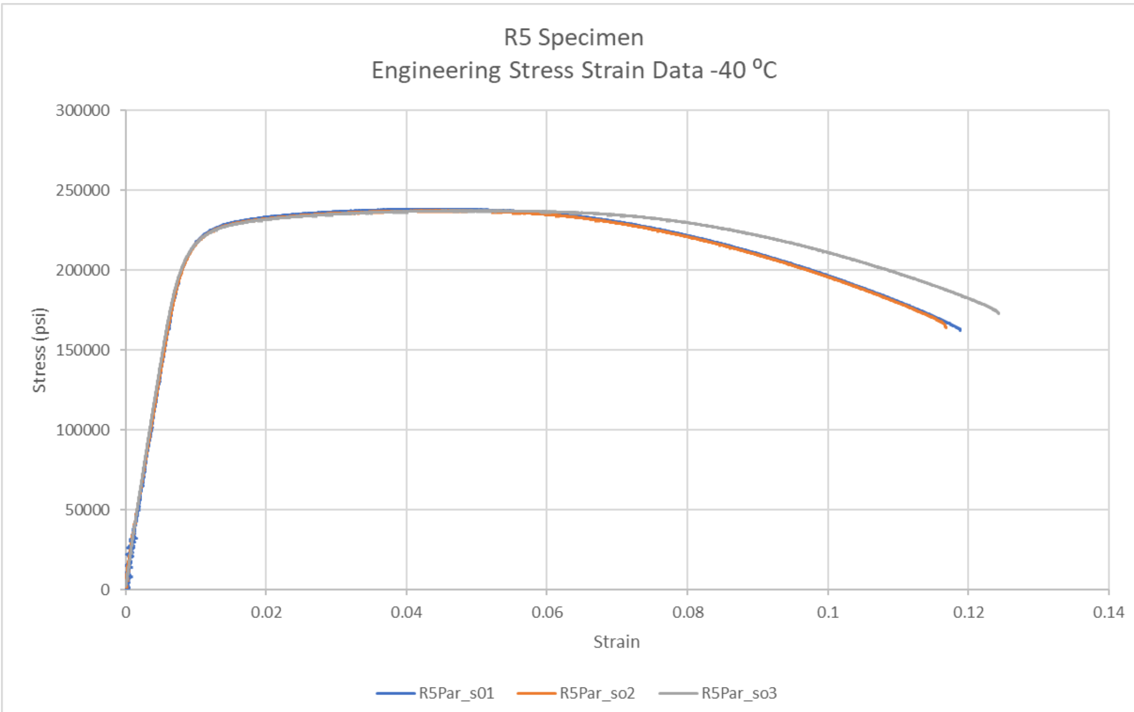

Figure 6. Engineering stress-strain data for R5 tensile specimens tested at -40°C

A MATLAB script was written to develop the true stress-strain curve from the engineering stresss- strain data. The proportional limit was used in place of the yield stress because of the large gradual slope change from the initial linear elastic region of the curve to the ultimate stress peak. Using the proprotion limit versus the offset yield stress produces a true stress-strain curve that is more conservative and one that will result in higher plastic strains. Data for the three R5 test specimens derived using the MATLAB script are shown in Table 1.

Table 1 Test and calculated data from three -40°C tests

Specimen	Reduction in Area	Final Area (in^2)	Proportional Limit (psi)	Prop Limit strain	Modulus (psi)	UTS (psi)	UTS Strain	Final Plastic Strain
So1	0.601	0.003813	192894	0.007522	26271321	238390	0.044	0.9176
So2	0.516	0.00465	194618	0.007635	25976753	237463	0.0448	0.7263
S03	0.487	0.00493	181094	0.006653	27290268	237449	0.0473	0.6679

4. MODELING OF THE FRACTURE SPECIMENS

The test specimens were modeled using Sandia National Laboratories' Sierra-Presto/Adagio finite element code [10]. This is a Lagrangian, three-dimensional, implicit finite element code. The finite element model uses the Hydra Plasticity material model. This model uses the Hill yield surface and allows for anisotropic behavior, although isotropic hardening was assumed in the analyses. The model uses a tabular definition of the material's hardening behavior, with dependence on equivalent plastic strain and optional dependence on temperature and/or plastic strain rate. The Lode angle parameter, ξ, and the stress triaxiality η, are determined as part of the Hyper Plasticity model. Integration functions were added to the input file to calculate the average values of the parameters given in Equation (10 and 11 at each time step.

4.1 Specimens -40ºC

Engineering stress-strain curves for each of the three (-40ºC) R5 test specimens were run using the R5 FEA model. The force-displacement curves from the three models along with the FEA model results are shown in Figure 7. This shows very good agreement between the finite element models and the test specimen curves. This indicates that the model is capturing the correct necking and plastic deformation (reduction in area) of the tensile specimens.

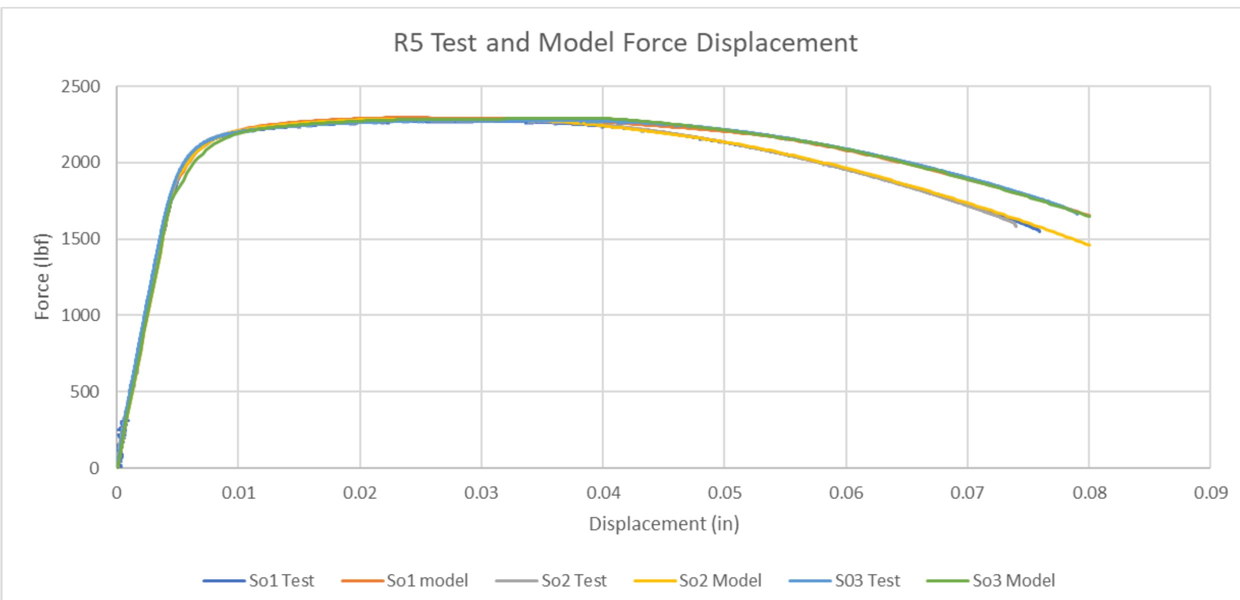

Figure 7 Comparison of -40ºC R5 test and model data

Using these results , the -40ºC true stress-strain curve shown in Figure 8 was chosen to model the PH13-8Mo H950 material. The MATLAB algoritm determines the slope of the curve using the six control points shown in Red.

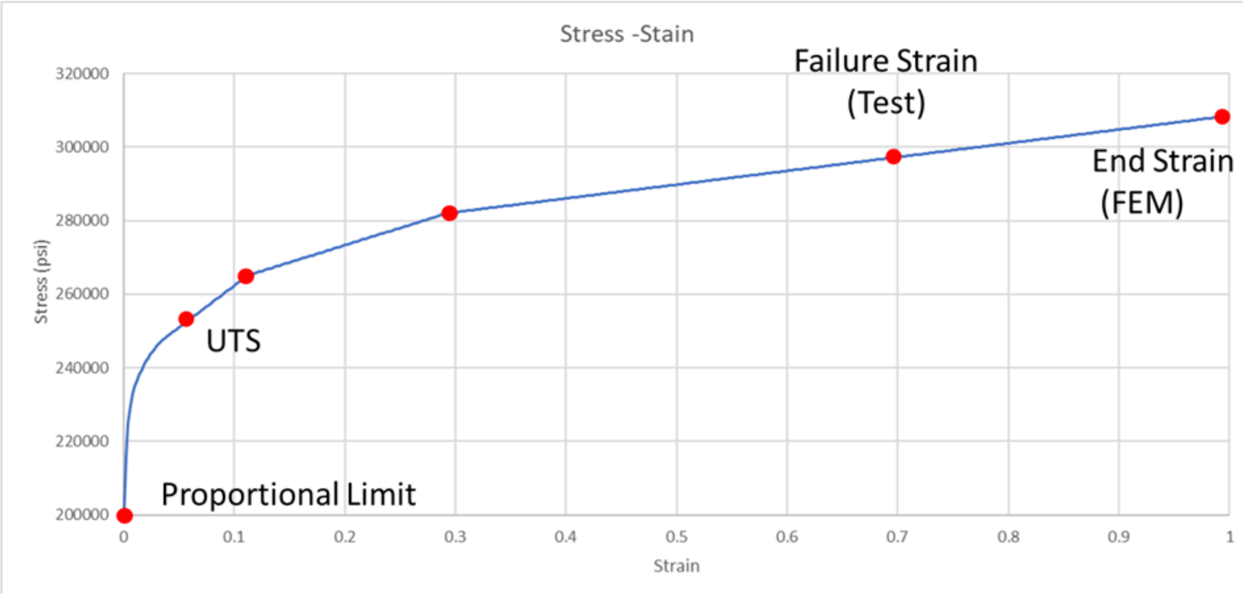

Figure 8. Final true stress-strain curve for -40°C along with the point used to in the MATLAB code.

The stress-strain curve in Figure 8 was incorporated into finite element models for each of the remaining test specimens. The force-displacement curves from each specimen along with the finite element results are shown in Figure 9-12 for the -40°C specimens. These curves show good agreement between the finite element models and the test data, particularly the axisymmetric models ($\xi = 1$). The flat bar and shear specimen show opposite hardening behaviors. The flat bar specimen is slightly harder than the model (high hardening and peak load). While the shear specimen shows a lower peak load and hardening curve. The displacements at fracture for each test specimen will be used to determine the final state of the material using the finite element model.

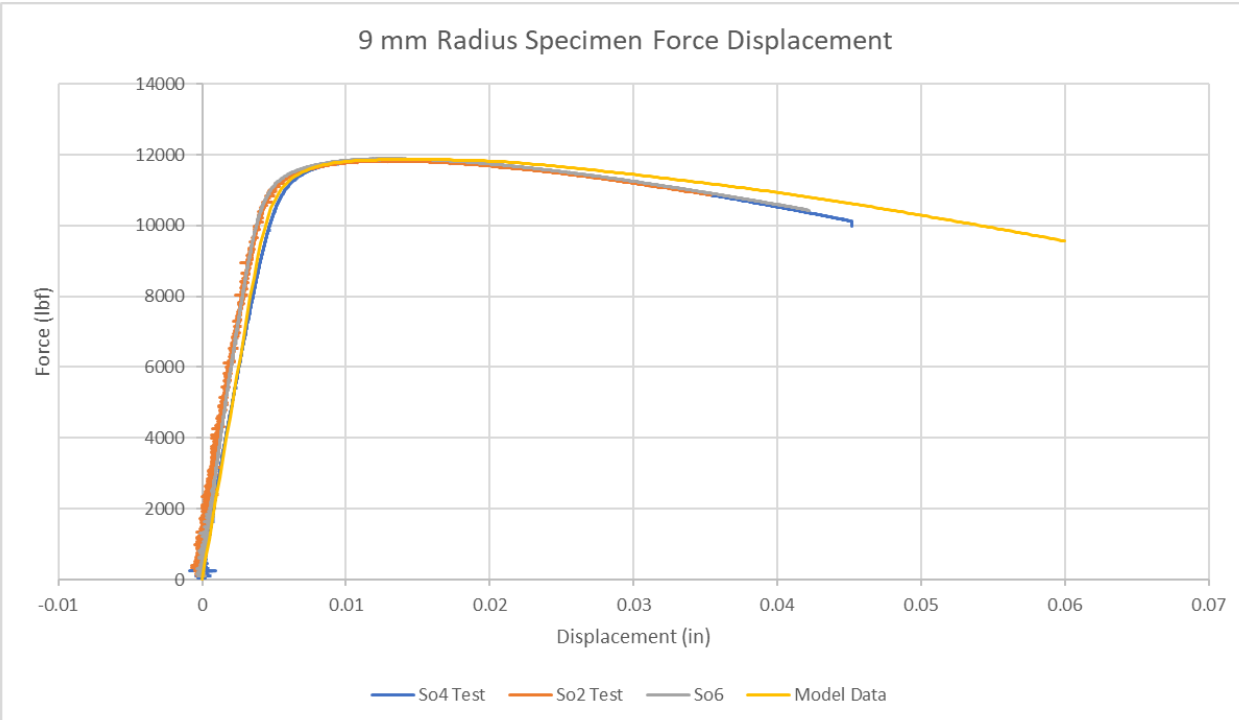

Figure 9. Comparison of the -40^{o}C R9 test specimen and model data

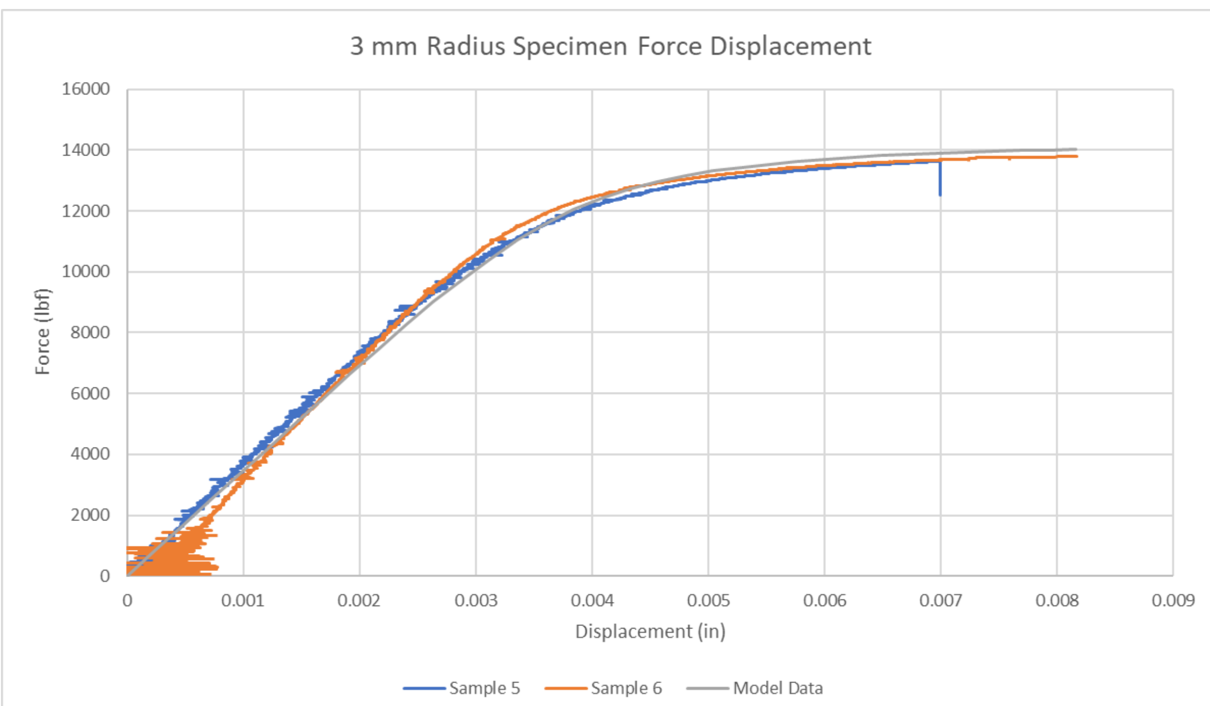

Figure 10. Comparison of the -40^{o}C R3 specimen tests and model data

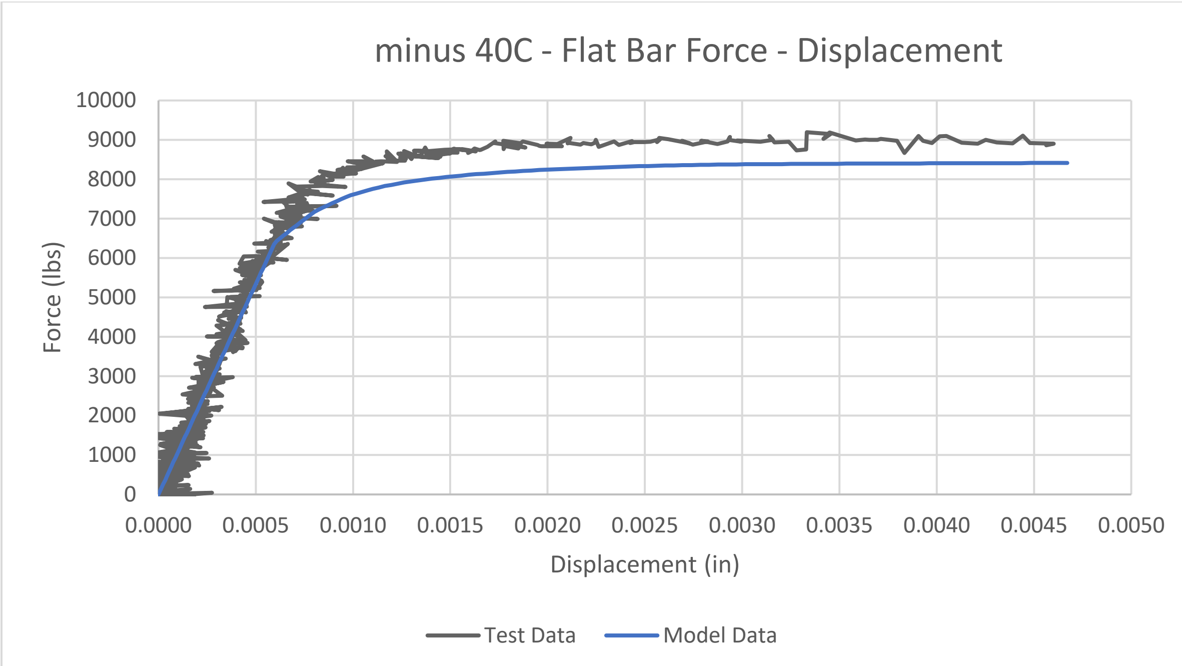

Figure 11. Comparison of the -40°C flat bar specimen test and model data

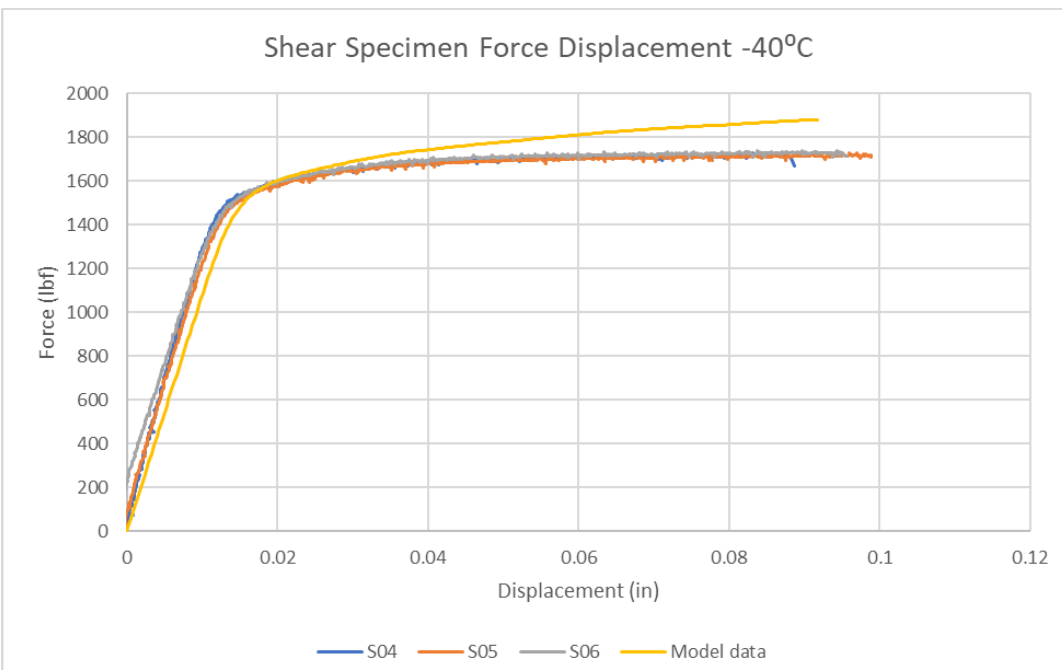

Figure 12. Comparison of the -40°C shear specimen tests and model data

4.2 Specimens 20°C

Using the same MATLAB algorithm and the data from the three 20°C R5 tensile tests, the stress-strain curve shown in Figure 13 was developed. Using this curve, the analyses of the five specimens tested at 20ºC were performed. The results of these analyses are compared to their respective test specimens in Figures 14 –17. As in the lower temperature test, the axisymmetric models show good agreement with the test data. The flat bar and shear specimens show the same behavior as the low temperature specimens with the flat bar specimen having a higher load profile and the shear specimen a lower load profile than their respective finite element models.

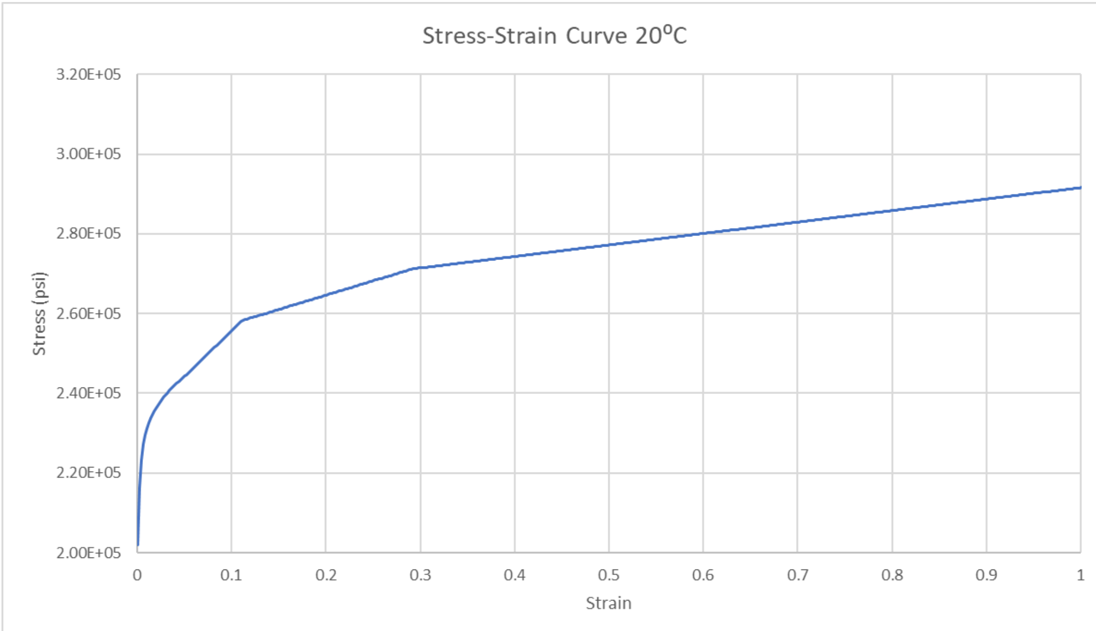

Figure 13. Stress-Strain curve from 20ºC R5 Specimens

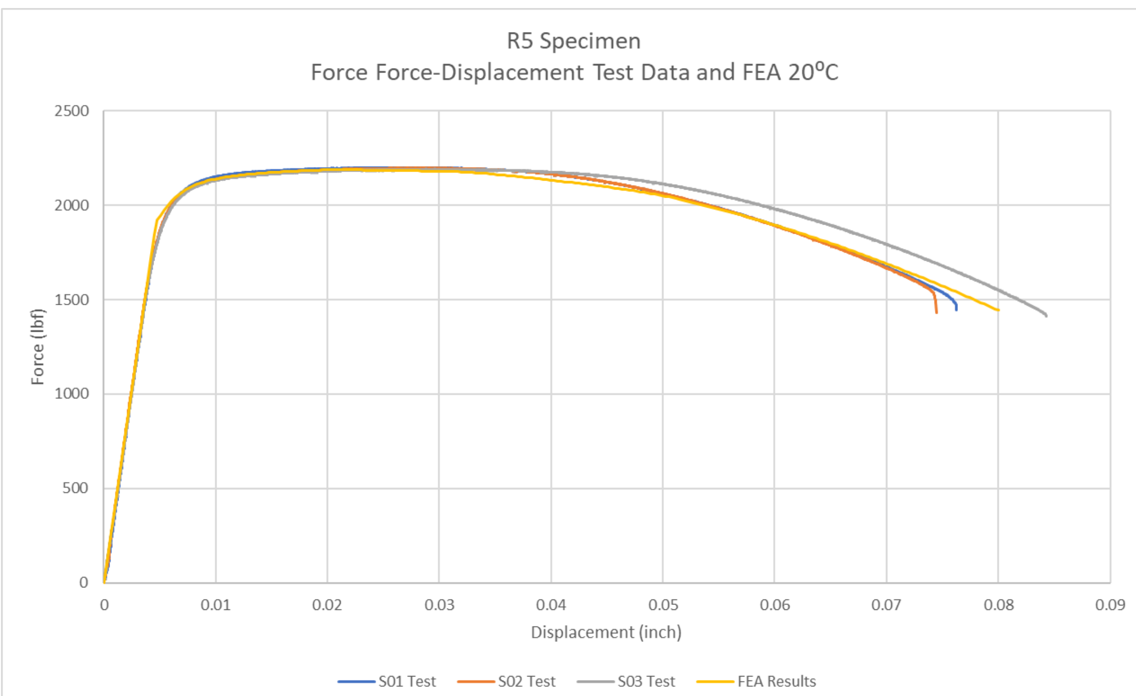

Figure 14. Comparison of 20ºC R5 test and model data.

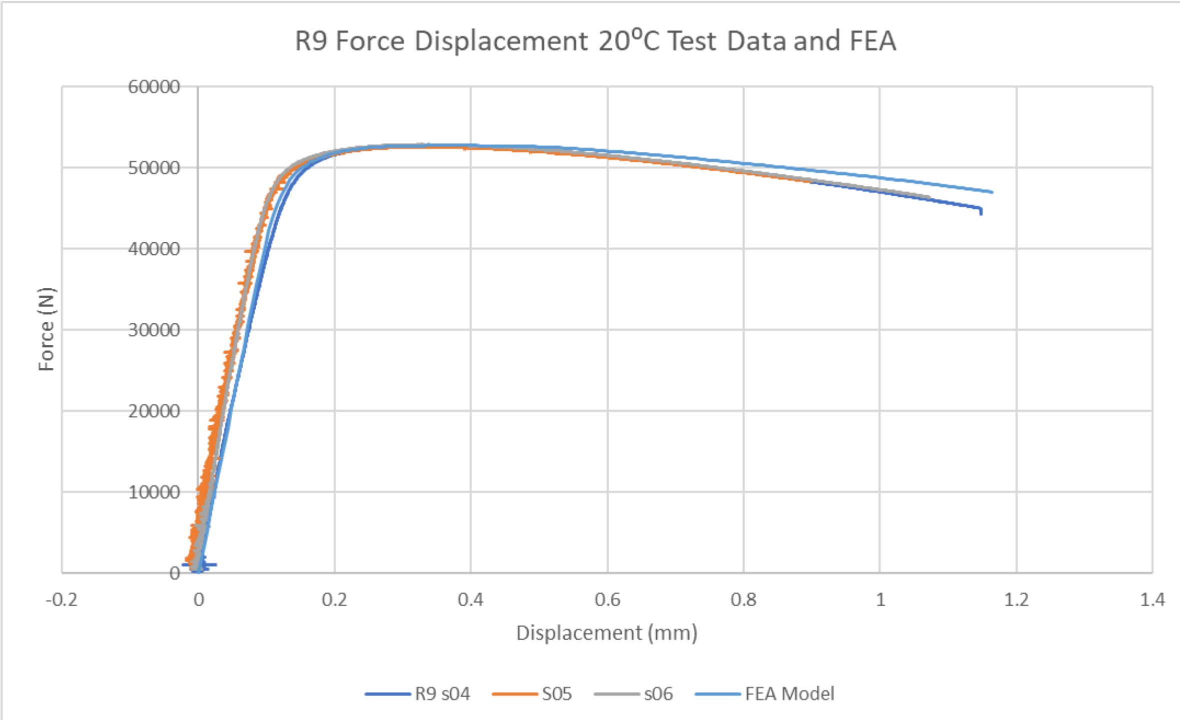

Figure 15. Comparison of the 20ºC R9 test specimen and model data

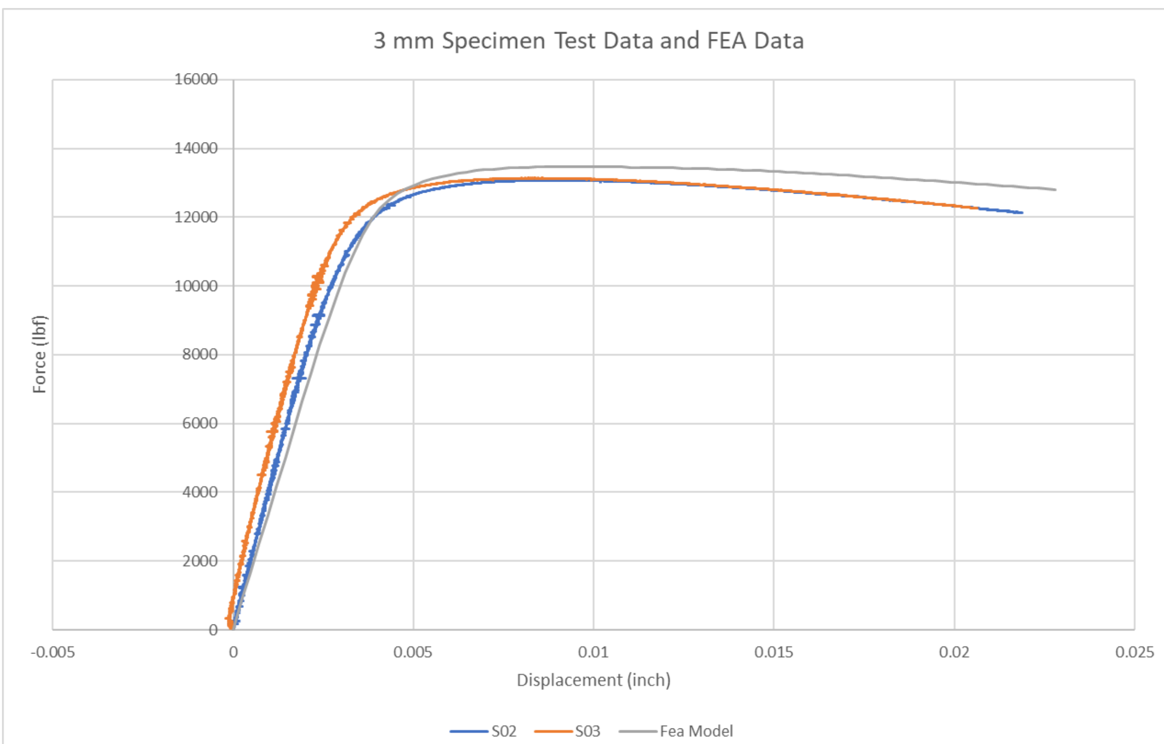

Figure 16. Comparison of the 20ºC R3 specimen tests and model data

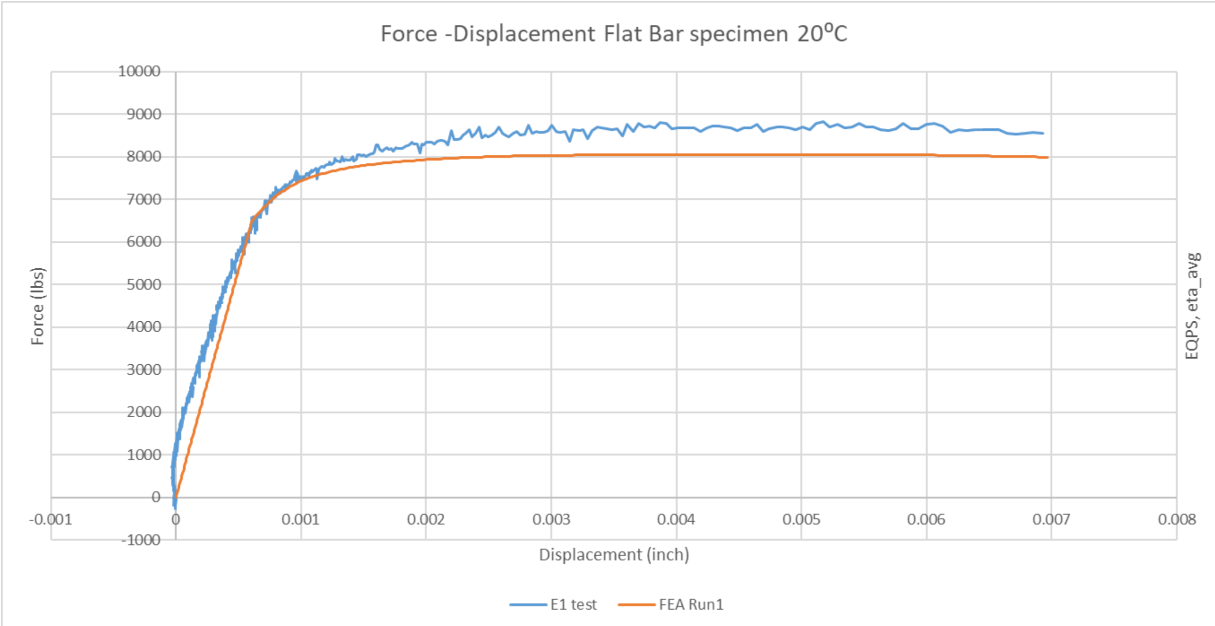

Figure 17 Comparison of the 20⁰C flat bar specimen test and model data

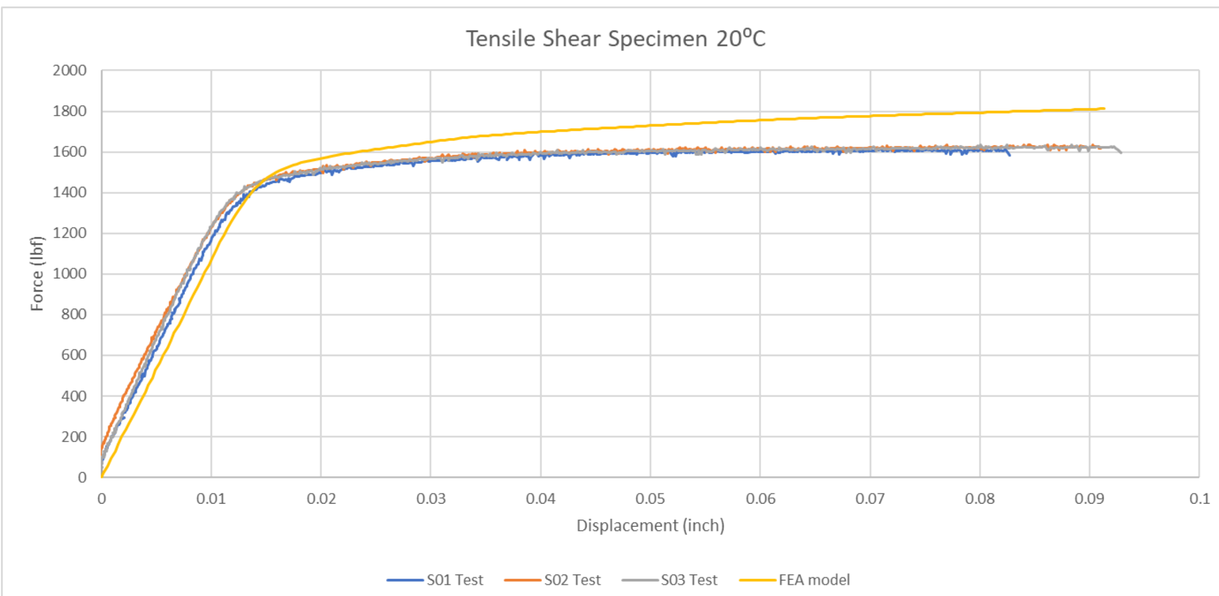

Figure 18. Comparison of the -40⁰C shear specimen tests and model data

5. DETERMINING THE FAILURE SURFACE

The data from the finite element models were used to determine the stress state in the specimens at fracture. The peak plastic strain and the corresponding values of the average stress triaxiality (η) and Lode angle parameter (ξ) were determined when the displacement of the finite element model matched the lowest failure displacement of a corresponding test specimen, Those values are given in Table 2.

Table 2. Test specimen failure data calculated using finite element models

Specimen	Temperature	EQPS	η	ξ
R5	-40°C	0.867283	0.604568	1
R9	-40°C	0.295864	0.75659	1
R3	-40°C	0.01821	0.877645	1
Flat bar	-40°C	0.07844	0.555739	0
Shear Specimen	-40°C	0.488043	0.003294	0
R5	20°C	0.892369	0.592633	1
R9	20°C	0.520324	0.784654	1
R3	20°C	0.189731	1.09467	1
Flat bar	20°C	0.194358	0.578298	0
Shear Specimen	20°C	0.474617	0.003082	0

Using the values from Table 2, the coefficients for Equation (12) and Equation (12) can be calculated. The values for these parameters are given in Table 3.

Table 3. Equation parameters calculated from finite element data

Specimen	Temperature	Constant	Value
R5 and R3	-40°C	C2	14.148
R5 and R3	-40°C	C1	4495.605
Flat bar and shear	-40°C	C3	0.488
Flat bar and Shear	-40°C	C4	3.289
R5 and R3	20°C	C2	3.084
R5 and R3	20°C	C1	5.550
Flat bar and shear	20°C	C3	0.475
Flat bar and shear	20°C	C4	1.544

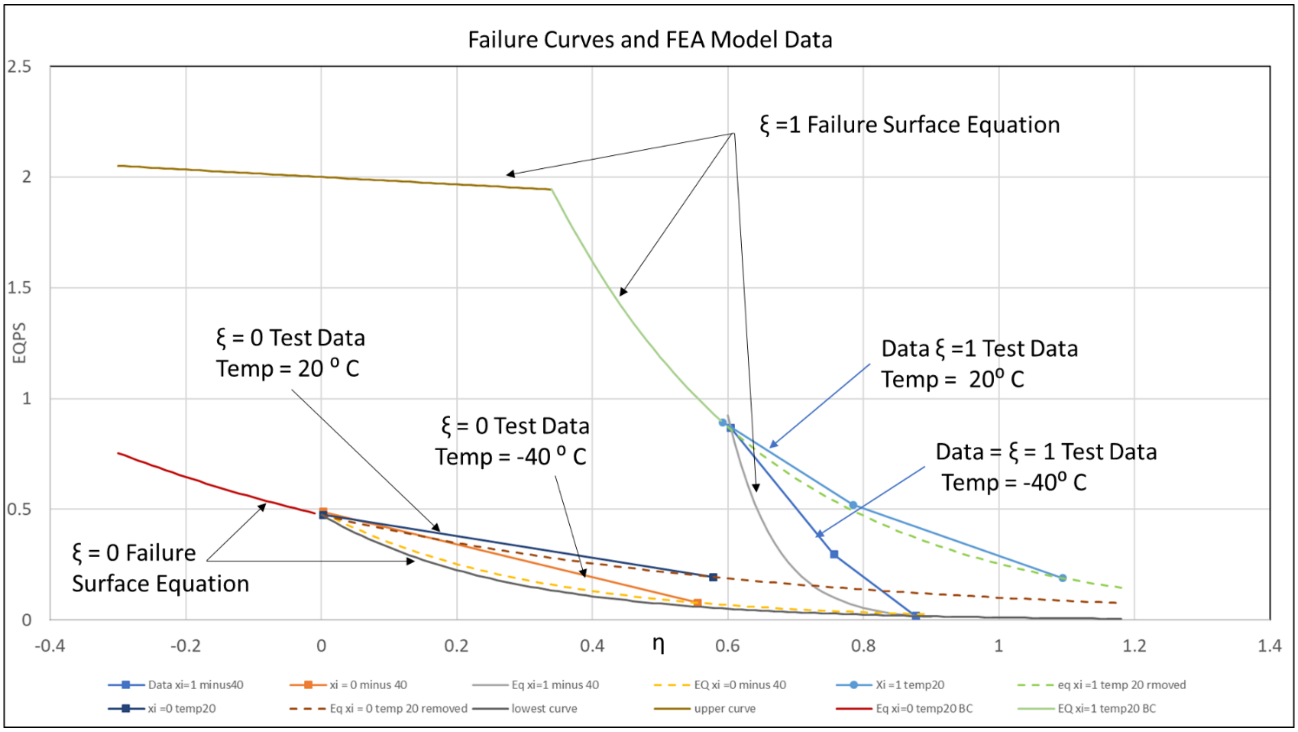

Figure 19. Plot of failure data from Table 1 and Table 2.

Figure 19 is a 2-D plot of Equations 12 and 13 using the constants from Table 3 along with the FEA data from Table 2. The plot shows the upper and lower bounding curve for $\xi = 1$ and $\xi = 0$. The $\xi = 1$ failure surface is defined by the gray, green, and brown curves. The gray curve is defined by the coefficients C_1 and C_2 for the -40°C, R5 and 3mm radius specimens. The dashed green curve is defined using the coefficients C_1 and the C_2 for the R5, and 3mm radius 20°C specimen. The solid green curve is an extension of the green dashed curve.

The -40°C and 20°C R5 specimens failed at very similar values of EQPS and η when $\eta < 0.6$. However, there is a very sharp drop in the failure strain of the -40°C specimen at value of $\eta >$ 0.6. Since the exponential equation approximation uses only two coefficients, the equation derived using the data from the -40°C R5 and 3mm specimens has a steep negative slope to the right of the point $\eta = 0.6$ (gray curve). While this curve goes through the R5 and 3mm radius data points, it results in a substantial difference in the failure strain between the -40°C 9mm test data point and the equation approximation. For the 9mm specimen, the equation value is approximately 1/3 of the test specimen failure strain. If an exponential least square fit was used with all three points, the resulting curve would be above the 3 mm data point and not properly capture that failure strain. Therefore, the two endpoints are used (R5, 3mm) and this results in a more conservation approximation of failure for in the range $0.6 < \eta < 0.87$.

The failure strains for the 20°C R5, 9mm radius, and 3mm radius specimens decreases at a lower rate with increased values of the stress triaxiality This results in a lower slope of the curve and a better approximation of the test data by the exponential function (green dashed curve). For values of $\eta < 0.6$ the lower slope of the 20°C curve results in lower estimates for the failure strain and therefore is a more conservative approximation for the failure surface. Thus, the solid green curve is taken as the upper limit of failure for $\xi = 1$ for values of $\eta < 0.6$. The brown curve for the $\xi = 1$ failure surface was added to limit the peak values for plotting.

The $\xi = 0$ failure surface is defined by the black, and red curves. The 20ºC and -40ºC curves have similar failure strains in simple shear ($\eta = 0$). There is a drop in the -40ºC curve compared to the 20ºC curve for values of $\eta > 0$. To produce the most conservative curve, the lower black curve is derived using the points from the -40ºC shear specimen and the -40ºC, 3mm radius specimen. Similar to the $\xi = 1$ failure surface, the failure surface for values of $\eta < 0$ follow the lower slope, 20ºC curve (red curve).

Using Equation 14, a 3-D plot of the failure surface is shown in Figure 20. The hardening parameter *1/n* was determined by fitting an exponential curve to the curve in Figure 8. The value of *m* was set equal to 8. The failure surface shows a very steep increase in failure strain at the limit of $\xi = \pm 1$. There are also very small failure strains at high stress triaxialities independent of the Lode parameter.

The integration of the stress state can be carried out during the analysis and element stress state can be compared to the derived failure surface to determine element failure or the failure surface can be used as a post processing failure check to prove design robustness.

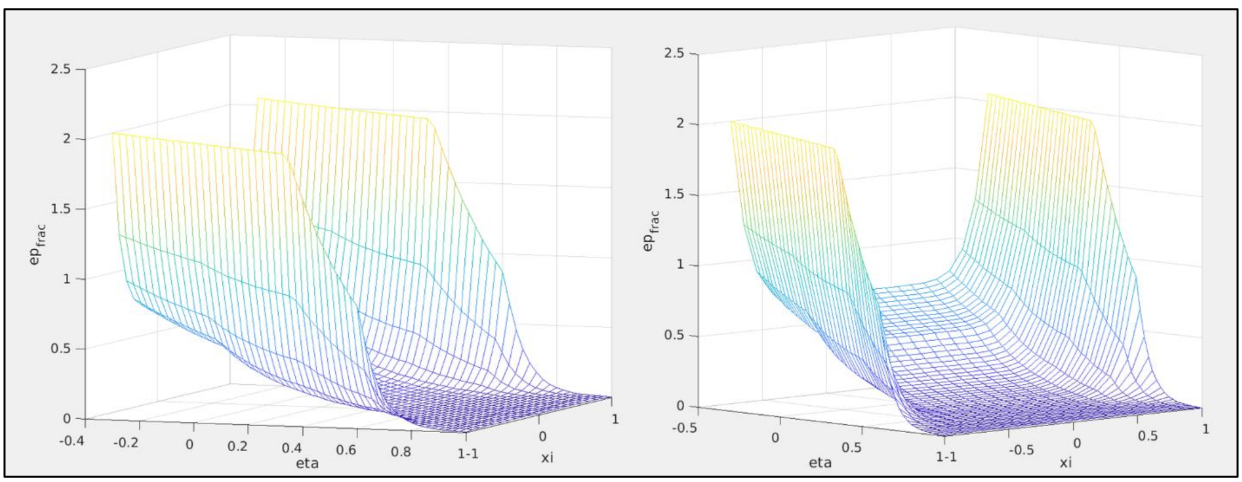

Figure 20. 3-D plot of failure surface.

6. CONCLUSION

A failure surface was developed for PH13-8Mo H950 steel using the Xue-Wierzbicki failure model based on equivalent plastic strain, stress triaxiality, and Lode angle. Five types of tensile specimens were tested with Lode angle parameters of 1 and 0 at -40°C and 20°C. Finite element models of the test specimens were used to determine the plastic strain, average stress triaxiality, and the average value of the Lode parameter at fracture. These parameters were then used to define the failure surface using the Xue-Wierzbicki form of the failure function. The failure surface can be used during the analysis to determine element death or as a post processing check.

REFERENCES

.

[1] Wierzbicki, T., et al., Calibration and evaluation of seven fracture models. International Journal of Mechanical Sciences, 2005. 47(4-5): p. 719-743

[2] Noell P.J., Pathare P.R., Casias Z., Huber T., Laing J., and Carrol J.D., Mechanical testing of PH13-8Mo H950 Steel for Xue-Wierzbicki Fracture Criterion Determination at 20° C and -40° C. Tech Rept. SAND2020-5906, Sandia National Laboratories.

[3] International, A., Standard Test Methods for Tension Testing of Metallic Materials. Standard Designation E8 -16, ASTM International, West Conshohocken, PA, 2016.

[4] Bridgman, P.W. (1964), "Studies in Large Plastic Flow and Fracture," Harvard University Press, Cambridge, Massachusetts.

[5] Johnson, G.R., and Cook, W.H., Fracture Characteristics of Three Metals Subjected to Various Strains, Strain Rates, Temperature and Pressures, Engineering Fracture Mechanics, 21, pp.31-48, 1985.

[6] Bao, Y., Prediction of Ductile Crack Formation in Uncracked Bodies, Report 100, 2003, Impact & Crash Worthiness Laboratory, MIT, Cambridge, MA.

[7] Bao, Y. and Weirzbicki, T., A new model of metal plasticity and fracture with pressure and Lode dependence, International Journal of Plasticity, 24, pp1071-1096, 2008.

[8] Wierzbicki, T. and Xue, L., On the effect of the third invariant of the stress deviator on ductile fracture, Report 136, 2005, Impact & Crash Worthiness Laboratory, MIT, Cambridge, MA.

[9] Xue, Liang, Ductile fracture modeling – Theory, experimental investigation and numerical verification, Massachusetts Institute of Technology, 2007

[10] SIERRA Solid Mechanics, Sierra/SolidMechanics 4.58 User's Guide, Technical Report, Sandia National Laboratories, Albuquerque, NM 87185-0380, Nov. 2020.

APPENDIX A. SPECIMEN DRAWINGS

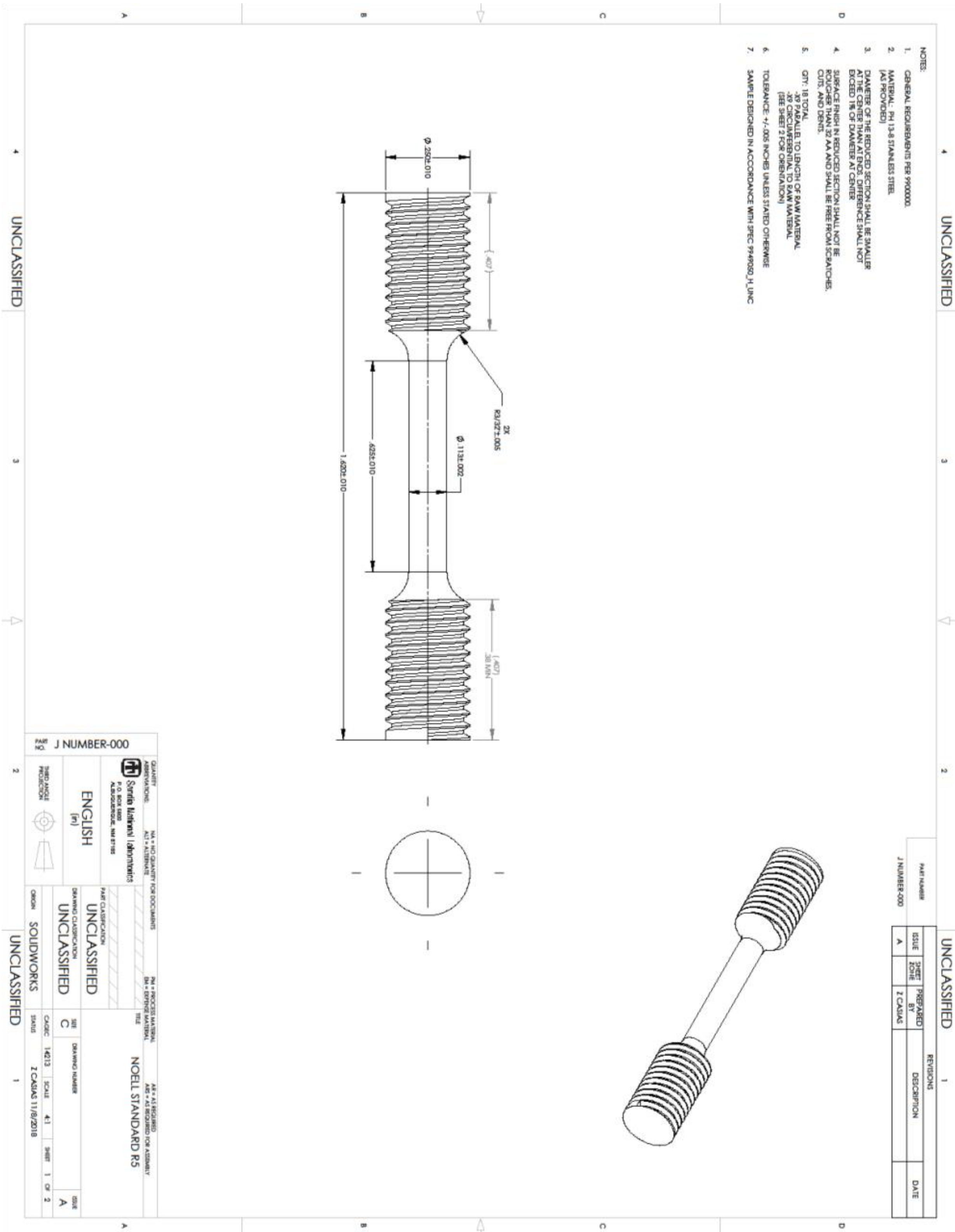

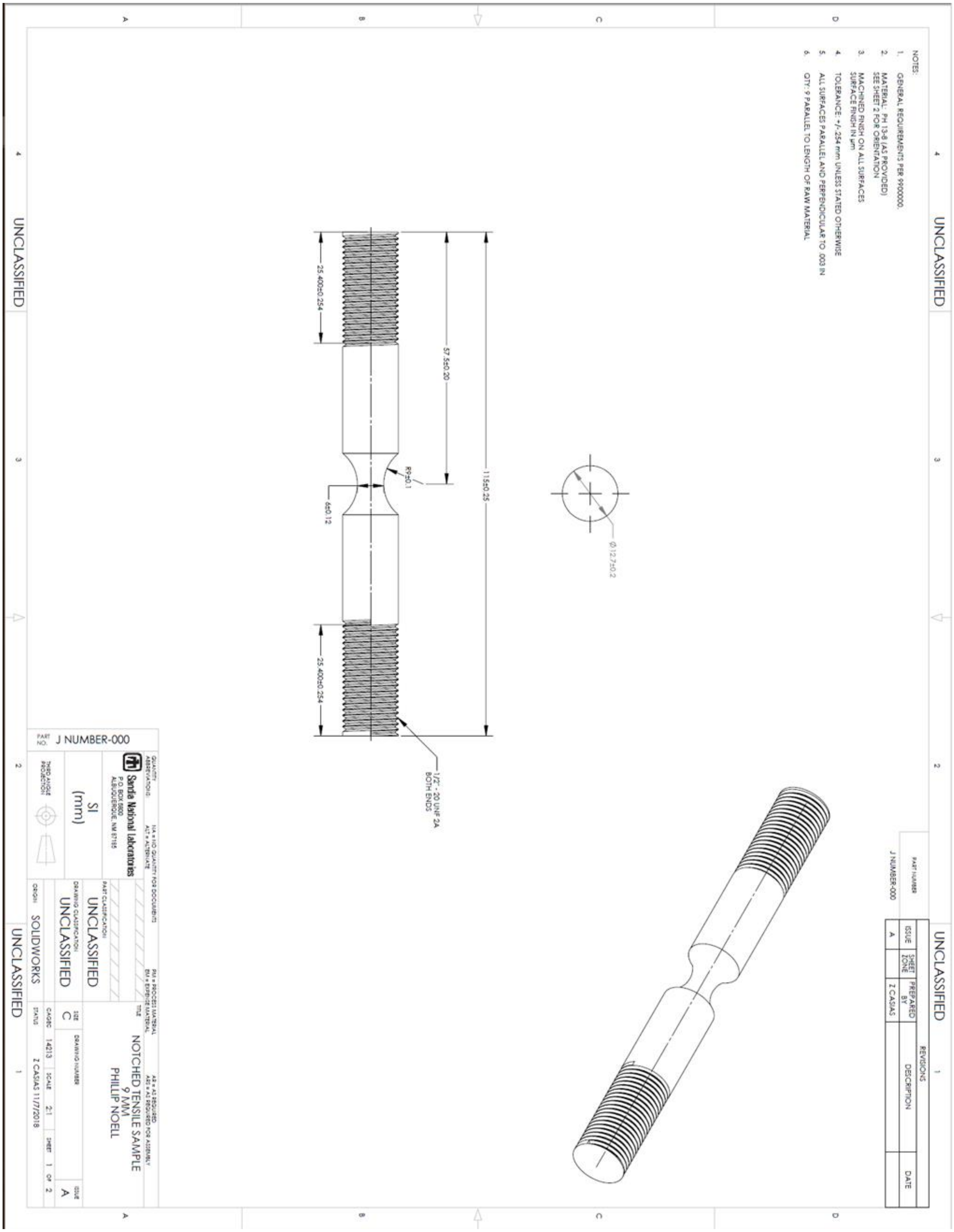
UNCLASSIFIED
NOTES:
1. GENERAL REQUIREMENTS PER 9900000.
2. MATERIAL: PH 13-8 (AS PROVIDED)
SEE SHEET 2 FOR ORIENTATION
3. MACHINED FINISH ON ALL SURFACES
SURFACE FINISH IN μm
4. TOLERANCE: +/-.254 mm UNLESS STATED OTHERWISE
5. ALL SURFACES PARALLEL AND PERPENDICULAR TO .003 IN
6. QTY: 9 PARALLEL TO LENGTH OF RAW MATERIAL
PART NUMBER
J NUMBER-000
REVISIONS
ISSUE
SHEET ZONE
PREPARED BY
DESCRIPTION
DATE
A
Z CASIAS
Ø12.7±0.2
115±0.25
57.5±0.20
R9±0.1
6±0.12
25.400±0.254
25.400±0.254
1/2" - 20 UNF 2A
BOTH ENDS
QUANTITY ABBREVIATIONS:
NA = NO QUANTITY FOR DOCUMENTS
ALT = ALTERNATE
PM = PROCESS MATERIAL
EM = EXPENSE MATERIAL
AR = AS REQUIRED
ARS = AS REQUIRED FOR ASSEMBLY
Sandia National Laboratories
P.O. BOX 5800
ALBUQUERQUE, NM 87185
TITLE
NOTCHED TENSILE SAMPLE
9 MM
PHILLIP NOELL
PART CLASSIFICATION
UNCLASSIFIED
SI
(mm)
DRAWING CLASSIFICATION
UNCLASSIFIED
SIZE
C
DRAWING NUMBER
ISSUE
A
PART NO. J NUMBER-000
THIRD ANGLE PROJECTION
CAGEC 14213
SCALE 2:1
SHEET 1 OF 2
ORIGIN SOLIDWORKS
STATUS Z CASIAS 11/7/2018
UNCLASSIFIED

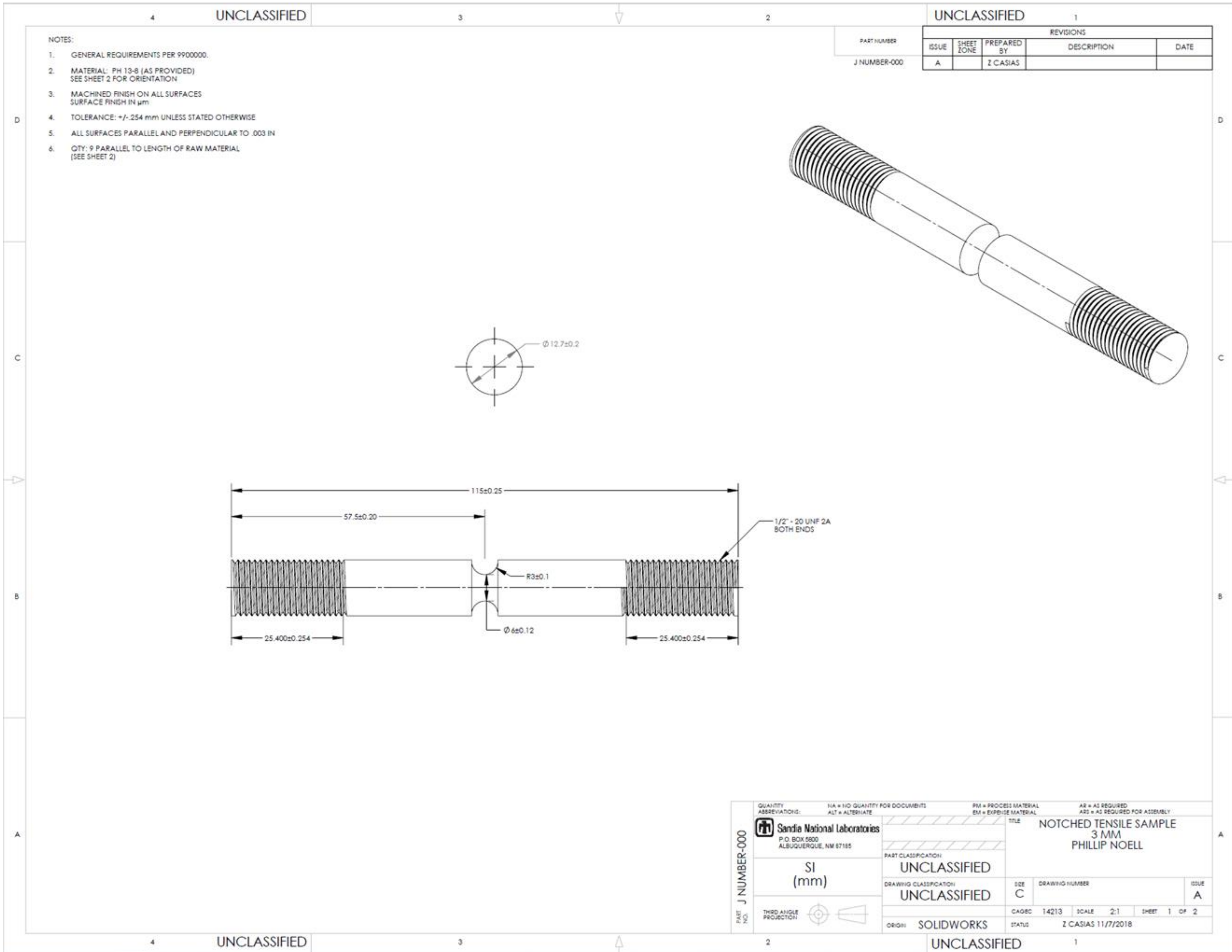
UNCLASSIFIED
NOTES:
1. GENERAL REQUIREMENTS PER 9900000.
2. MATERIAL: PH 13-8 (AS PROVIDED) SEE SHEET 2 FOR ORIENTATION
3. MACHINED FINISH ON ALL SURFACES SURFACE FINISH IN μm
4. TOLERANCE: +/-.254 mm UNLESS STATED OTHERWISE
5. ALL SURFACES PARALLEL AND PERPENDICULAR TO .003 IN
6. QTY: 9 PARALLEL TO LENGTH OF RAW MATERIAL (SEE SHEET 2)
PART NUMBER
J NUMBER-000
REVISIONS
ISSUE
SHEET ZONE
PREPARED BY
DESCRIPTION
DATE
A
Z CASIAS
Ø 12.7±0.2
115±0.25
57.5±0.20
1/2" - 20 UNF 2A BOTH ENDS
R3±0.1
Ø 6±0.12
25.400±0.254
25.400±0.254
QUANTITY ABBREVIATIONS: NA = NO QUANTITY FOR DOCUMENTS ALT = ALTERNATE
PM = PROCESS MATERIAL EM = EXPENSE MATERIAL
AR = AS REQUIRED ARS = AS REQUIRED FOR ASSEMBLY
Sandia National Laboratories
P.O. BOX 5800
ALBUQUERQUE, NM 87185
TITLE
NOTCHED TENSILE SAMPLE
3 MM
PHILLIP NOELL
SI
(mm)
PART CLASSIFICATION
UNCLASSIFIED
DRAWING CLASSIFICATION
UNCLASSIFIED
SIZE
C
DRAWING NUMBER
ISSUE
A
PART NO. J NUMBER-000
THIRD ANGLE PROJECTION
CAGEC 14213
SCALE 2:1
SHEET 1 OF 2
ORIGIN SOLIDWORKS
STATUS Z CASIAS 11/7/2018
UNCLASSIFIED

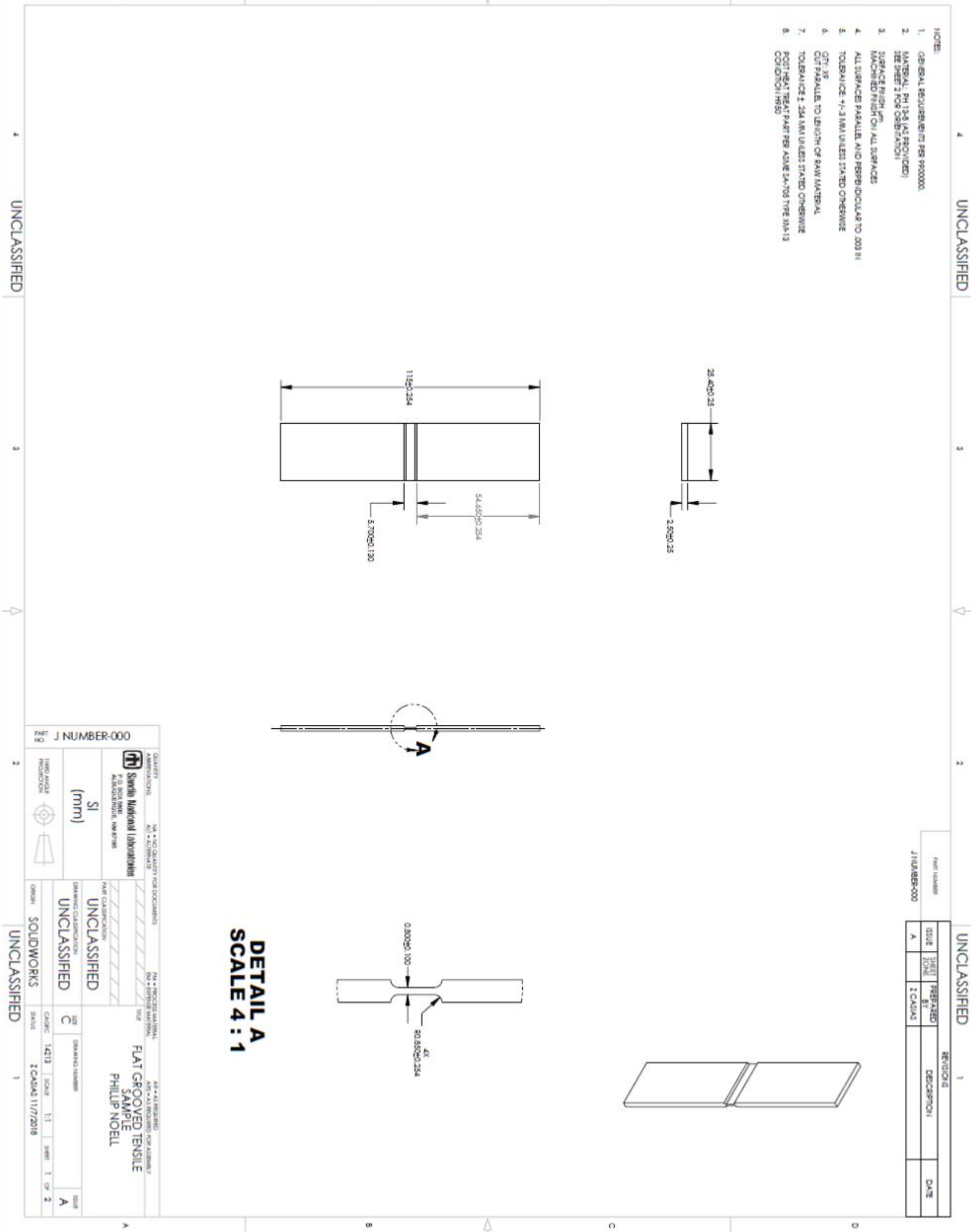
UNCLASSIFIED
NOTES:
3. SURFACE FINISH µm
MACHINED FINISH ON ALL SURFACES
4. ALL SURFACES PARALLEL AND PERPENDICULAR TO .003 IN
5. TOLERANCE +/-.3 MM UNLESS STATED OTHERWISE
6. QTY: X9
CUT PARALLEL TO LENGTH OF RAW MATERIAL
7. TOLERANCE ± .254 MM UNLESS STATED OTHERWISE
8. POST HEAT TREAT PART PER ASME SA-705 TYPE XM-13
CONDITION H950
115±0.254
54.650±0.254
5.700±0.130
25.40±0.25
2.50±0.25
A
DETAIL A
SCALE 4 : 1
0.800±0.100
4X
R0.850±0.254
PART NO. J NUMBER-000
Sandia National Laboratories
P.O. BOX 5800
ALBUQUERQUE, NM 87185
SI
(mm)
THIRD ANGLE PROJECTION
PART CLASSIFICATION
UNCLASSIFIED
DRAWING CLASSIFICATION
UNCLASSIFIED
ORIGIN SOLIDWORKS
TITLE
FLAT GROOVED TENSILE
SAMPLE
PHILLIP NOELL
SIZE C
DRAWING NUMBER
ISSUE A
CAGEC 14213
SCALE 1:1
SHEET 1 OF 2
STATUS Z CASIAS 11/7/2018
PART NUMBER
J NUMBER-000
REVISIONS
ISSUE
SHEET ZONE
PREPARED BY
DESCRIPTION
DATE
A
Z CASIAS

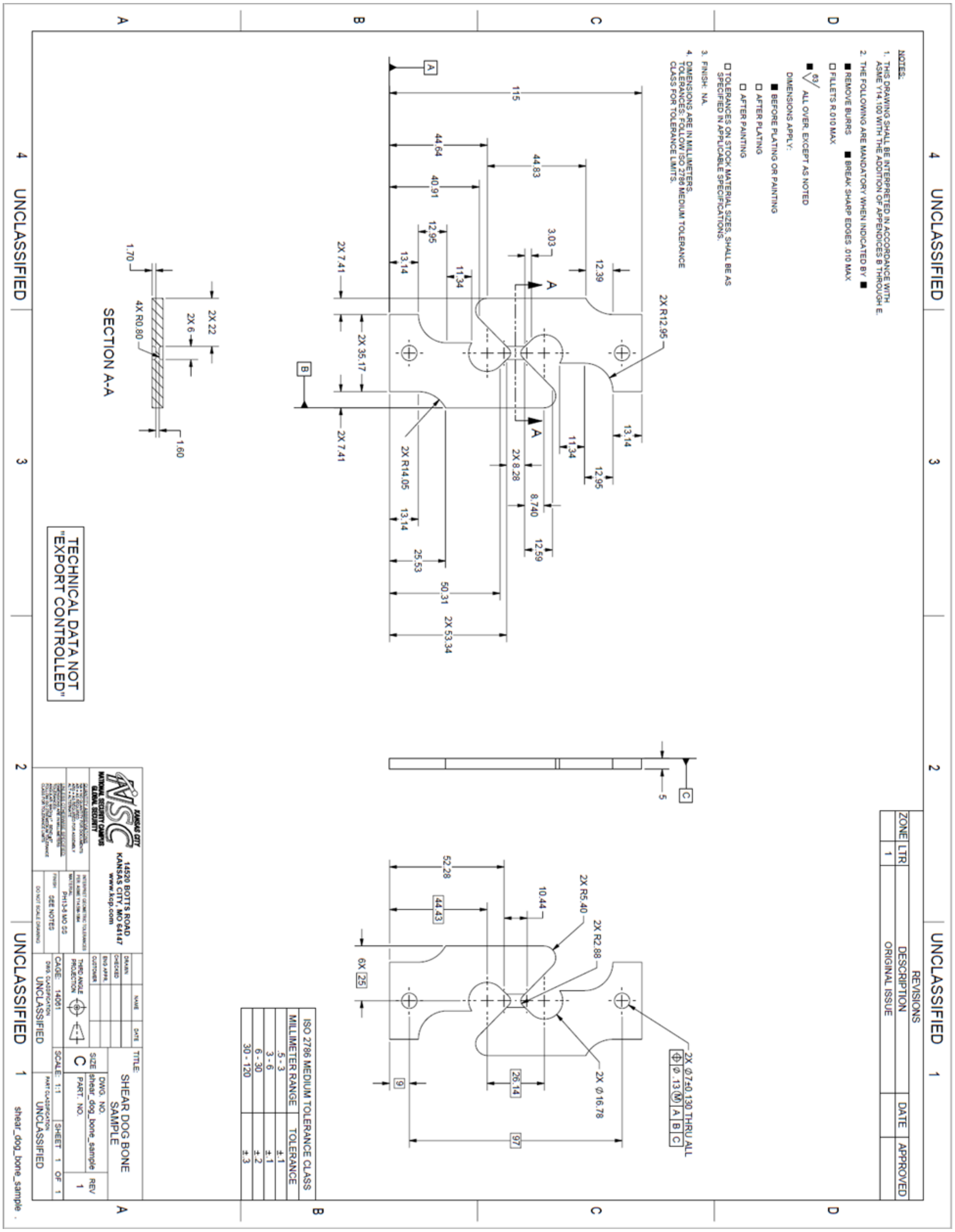
UNCLASSIFIED
NOTES:
1. THIS DRAWING SHALL BE INTERPRETED IN ACCORDANCE WITH ASME Y14.100 WITH THE ADDITION OF APPENDICES B THROUGH E.
2. THE FOLLOWING ARE MANDATORY WHEN INDICATED BY ■
■ REMOVE BURRS ■ BREAK SHARP EDGES .010 MAX
□ FILLETS R.010 MAX
■ 63 ALL OVER, EXCEPT AS NOTED
DIMENSIONS APPLY:
■ BEFORE PLATING OR PAINTING
□ AFTER PLATING
□ AFTER PAINTING
□ TOLERANCES ON STOCK MATERIAL SIZES, SHALL BE AS SPECIFIED IN APPLICABLE SPECIFICATIONS.
3. FINISH: NA.
4. DIMENSIONS ARE IN MILLIMETERS. TOLERANCES: FOLLOW ISO 2786 MEDIUM TOLERANCE CLASS FOR TOLERANCE LIMITS.
SECTION A-A
TECHNICAL DATA NOT "EXPORT CONTROLLED"
REVISIONS
ZONE
LTR
DESCRIPTION
DATE
APPROVED
1
ORIGINAL ISSUE
ISO 2786 MEDIUM TOLERANCE CLASS
MILLIMETER RANGE
TOLERANCE
.5 - 3
±.1
3 - 6
±.1
6 - 30
±.2
30 - 120
±.3
KANSAS CITY NATIONAL SECURITY CAMPUS
14520 BOTTS ROAD KANSAS CITY, MO 64147 www.kcp.com
TITLE: SHEAR DOG BONE SAMPLE
SIZE C
DWG. NO. shear_dog_bone_sample
REV 1
SCALE: 1:1
SHEET 1 OF 1
MATERIAL PH13-8 MO SS
FINISH SEE NOTES
CAGE: 14061
UNCLASSIFIED
shear_dog_bone_sample

DISTRIBUTION

Email—Internal

Name	Org.	Sandia Email Address
D. J. Ammerman	8850	djammer@sandia.gov
G. J. Flores	8854	gjflore@sandia.gov
R. J. Kalan	8854	rjkalan@sandia.gov
S. E. Sanborn	8854	sesanbo@sandia.gov
Technical Library	01977	sanddocs@sandia.gov

This page left blank

This page left blank

Sandia National Laboratories is a multimission laboratory managed and operated by National Technology & Engineering Solutions of Sandia LLC, a wholly owned subsidiary of Honeywell International Inc. for the U.S. Department of Energy's National Nuclear Security Administration under contract DE-NA0003525.